NASA Technical Memorandum 106889
AIAA–95–1101

A Coupled Layerwise Analysis of the Thermopiezoelectric Response of Smart Composite Beams

H.-J. Lee
Lewis Research Center
Cleveland, Ohio

and

D.A. Saravanos
Ohio Aerospace Institute
Cleveland, Ohio

Prepared for the
36th Structures, Structural Dynamics, and Materials Conference
cosponsored by AIAA, ASME, AHS, and ASC
New Orleans, Louisiana, April 10–13, 1995

National Aeronautics and
Space Administration

A Coupled Layerwise Analysis of the Thermopiezoelectric Response of Smart Composite Beams

H.-J. Lee
National Aeronautics and Space Administration
Lewis Research Center
Cleveland, Ohio 44135

and

D.A. Saravanos*
Ohio Aerospace Institute
Brook Park, Ohio 44142

Abstract

Thermal effects are incorporated into previously developed discrete layer mechanics for piezoelectric composite beam structures. The updated mechanics explicitly account for the complete coupled thermoelectromechanical response of smart composite beams. This unified representation leads to an inherent capability to model both the sensory and actuator responses of piezoelectric composite beams in a thermal environment. Finite element equations are developed and numerical results are presented to demonstrate the capability of the current formulation to represent the behavior of both sensory and active smart structures under thermal loadings.

Introduction

The development of intelligent and smart composite materials with piezoelectric components offers great potential for use in advanced aerospace structural applications. This potential arises from two basic characteristics of piezoelectric materials, called the direct and converse piezoelectric effects, which allow for their use as sensors and actuators in composite structures. In the direct piezoelectric effect, application of a mechanical force on the piezoelectric material leads to the induction of an electrical charge or voltage, while in the converse piezoelectric effect the application of a charge or voltage produces a mechanical force or strain in the piezoelectric material. By taking advantage of the direct and converse piezoelectric effect of embedded piezoceramic or piezopolymer

*NASA Resident Research Associate at Lewis Research Center.

devices, these novel materials can combine the superior mechanical and thermal properties found in conventional composites along with the inherent self-monitoring and adaptive capabilities of piezoelectric materials. An area where such materials may provide dramatic advantages is in the development of smart composite structures with the capability to sense thermally induced distortions and to actively compensate for adverse thermomechanical conditions. Typical applications of such structures are envisioned in the thermal distortion management of propulsion components and/or space structures. However, before they can be utilized in these applications the performance of smart piezoelectric structures in thermal environments must be quantified. Consequently, this paper will present the development of comprehensive mechanics for the analysis of such smart thermal composite structures.

Extensive development of analytical methods for modeling the behavior of piezoelectric structures has been reported in the literature. The early works focused mainly on the development of simplified models for the vibration control of beams [Bailey and Hubbard (1985), Crawley and deLuis (1987)]. This was followed by the extension of classical lamination theory to incorporate piezoelectric effects [Tzou and Gadre (1989), Lee and co-workers (1991), Wang and Rogers (1991)]. The development of this piezoelectric laminate theory lead in turn to the formation of finite element methods for the analysis of smart structures using plate and shell elements [Allik and Hughes (1970), Naillon and co-workers (1983), Tzou and Tseng (1990), Lammering (1991), Ha and co-workers (1992)]. However, since classical lamination theory has been shown to have certain limitations in the analysis of thick or heterogenous (through-the-thickness) laminates [Reddy (1987)], a discrete layer theory for active beams based on an induced strain approach was implemented by Robbins and Reddy (1991) into a finite element formulation. This discrete layer theory was in turn extended to incorporate the coupled equations of piezoelectricity and developed into a multi-field formulation for beam and plate finite element equations by Heyliger, Ramirez & Saravanos (1993) and Saravanos & Heyliger (1994).

All of the previously described methods neglect the implications of thermal effects on both the active and sensory response of smart structures. Thermal effects become important when the piezoelectric structure has to operate in either extremely hot or cold temperature environments. These extreme conditions may severely affect the response of smart structures in three distinct ways: (1) induction of thermal stresses due to differences in the coefficients of thermal expansion between the various composite plies and piezoelectric layers, (2) pyroelectric phenomena (i.e. changes in the electrical displacements arising from the coupled electrical and thermal behavior of the piezoelectric material), and (3) temperature dependence of the elastic, piezoelectric, and dielectric properties. Only a limited amount of work has been reported concerning this topic.

Mindlin (1974) formulated a set of two-dimensional thermopiezoelectric equations for plates. Tauchert (1992) extended classical lamination theory to account for the coupled effects of thermopiezoelectricity. Rao and Sunar (1993), Tzou and Howard (1994), and Tzou and Ye (1994) developed finite element formulations for plates and shells (based on classical lamination theory) to account for thermopiezoelectricity.

Consequently, the purpose of this paper is to extend the previously developed discrete layer formulation of Saravanos and Heyliger (1994) to account for the coupled mechanical, electrical, and thermal response in modern smart composite beams. The mechanics account for thermal effects which may arise in the elastic and piezoelectric media at the material level through the constitutive equations. The displacements, electric potentials, and temperatures are introduced as state variables, allowing them to be modelled as variable fields through the laminate thickness. This unified representation leads to an inherent capability to model both the active compensation of thermal distortions in smart structures and the resultant sensory voltage when thermal loads are applied. The corresponding finite element formulation is developed, and numerical results demonstrate the ability to model both the active and sensory modes of composite beams with heterogeneous plies with an attached piezoelectric layer under thermal loadings.

Governing Material Equations

This section outlines the foundations and steps required for developing the governing equations of composite beams with embedded piezoelectric layers. The mechanical response of the piezoelectric material can be represented by the equation of motion

$$\rho \ \ddot{u}_i = \sigma_{ij,j} + \bar{f}_i \tag{1}$$

where ρ, $\ddot{u}_i$, u_i, σ_{ij}, $\bar{f}_i$ are the density, acceleration, displacement, stress, and body force per unit volume, respectively; with i, j ranging from 1 to 3.

The electrical response of the piezoelectric material is described by the electrostatic (or Maxwell's) equation

$$D_{i,i} = 0 \tag{2}$$

where D_i is the electric displacement.

The small deformation strain-displacement relations are

$$S_{ij} = \frac{1}{2} (u_{i,j} + u_{j,i}) \tag{3}$$

where S_{ij} is the strain tensor. The electric field vector E_i is related to the electric potential ϕ by

$$E_i = - \phi_{,i} \tag{4}$$

In the linear theory of piezoelectricity, the equations of elasticity are coupled to the equations of electrostatics. The constitutive equations for a thermopiezoelectric material [Nye (1964)] employing standard contracted notation are

$$S_\alpha = s_{\alpha\beta}^{E,T}(T)\ \sigma_\beta + d_{\alpha m}^{T}(T)\ E_m + \alpha_\alpha^{E,T}(T)\ \theta \tag{5}$$

$$D_m = d_{m\alpha}^{T}(T)\ \sigma_\alpha + e_{mk}^{\sigma,T}(T)\ E_k + p_m^{\sigma,T}(T)\ \theta \tag{6}$$

or in semi-inverted form

$$\sigma_\alpha = C_{\alpha\beta}^{E,T}(T)\ S_\beta - e_{\alpha m}^{T}(T)\ E_m - \lambda_\alpha^{E,T}(T)\ \theta \tag{7}$$

$$D_m = e_{m\alpha}^{T}(T)\ S_\alpha + e_{mk}^{S,T}(T)\ E_k + p_m^{S,T}(T)\ \theta \tag{8}$$

with,

$$\begin{aligned} e_{\alpha m}^{T}(T) &= C_{\alpha\beta}^{E,T}(T)\ d_{\beta m}^{T}(T) \\ \lambda_\alpha^{E,T}(T) &= C_{\alpha\beta}^{E,T}(T)\ \alpha_\beta^{E,T}(T) \\ \theta &= T - T_o \\ e_{mk}^{S,T}(T) &= e_{mk}^{\sigma,T}(T) - d_{m\alpha}^{T}(T)\ e_{\alpha k}^{T}(T) \\ p_m^{S,T}(T) &= p_m^{\sigma,T}(T) - d_{m\alpha}^{T}(T)\ \lambda_\alpha^{E,T}(T) \end{aligned} \tag{9}$$

where D_m is the electric displacement component; $C_{\alpha\beta}$ and $s_{\alpha\beta}$ are the elastic stiffness and compliance tensors; $d_{\alpha m}$ and $e_{\alpha m}$ are the different forms of the piezoelectric tensor; ϵ_{mk} is

the electric permittivity tensor; α_α and λ_α are the different forms of the coefficient of thermal expansion; p_m is the pyroelectric constant; θ is the temperature difference from the stress free reference temperature T_o to the current temperature T; superscripts E, σ, S, and T, represent constant voltage, constant stress, constant strain, and constant temperature conditions, respectively; α, β = 1, ..., 6; and k, m = 1, 2, 3.

Through use of the divergence theorem and neglecting body forces, Eqs. (1) and (2) can be expressed in an equivalent variational form as

$$\int_V \rho\, \ddot{u}_i\, \delta u_i\, dV + \int_V \sigma_{ij}\, \delta S_{ij}\, dV - \int_{V_p} D_i\, \delta E_i\, dV = \int_A \bar{t}_i\, \delta u_i\, dA + \int_{A_p} \bar{q}\, \delta\phi\, dA \tag{10}$$

where $\bar{t}_i$ are the surface tractions applied on the surface A; $\bar{q}$ is the electrical charge applied on the surface A_p of the piezoelectric material; V represents the whole volume including both composite and piezoelectric materials; and V_p represents the volume of the piezoelectric material only.

Discrete Layer Formulation

A discrete layer laminate theory for thermal piezoelectric composite beams is described in this section. For beams, a simplified displacement and electric potential can be obtained since only axial variations of the state variables are assumed

$$u = u(x,z)\ ,\quad v = 0\ ,\quad w = w(x,z)\ ,\quad \phi = \phi(x,z) \tag{11}$$

where x is the in-plane axis of the beam and z is the through-the-thickness axis.

The discrete layer theory implements the following piecewise continuous approximations through the laminate thickness for the state variables

$$u(x,z,t) = \sum_{j=1}^{n} U^j(x,t)\ \psi^j(z) \tag{12}$$

$$w(x,z,t) = \sum_{j=1}^{n} W^j(x,t)\ \psi_w^j(z) \tag{13}$$

$$\phi(x,z,t) = \sum_{j=1}^{n} \phi^j(x,t)\ \psi^j(z) \tag{14}$$

$$\theta(z,t) = \sum_{j=1}^{n} \theta^j(t)\ \psi^j(z) \tag{15}$$

where n is the number of interpolation functions ψ^j. For the case of constant through-the-thickness displacement [w(x,z,t) = w^o(x,t)], ψ_w^j is equal to unity. Currently, ψ^j is represented using linear Lagrangian interpolation functions. The simplified displacements and the assumption of constant through-the-thickness displacement leads to the simplified constitutive equations derived from Eqs. (5)-(8) shown in Appendix A.

By combining Eqs. (3), (7), (8), (10), (12)-(15) and integrating through-the-thickness, the following variational form can be obtained for the case of a constant through-the-thickness displacement beam

$$\begin{aligned}
&\sum_{k=1}^{n}\sum_{m=1}^{n} \int_x P_{11}^{km}\, \ddot{u}^m\, \delta u^k\, dx + \int_x P_{33}\, \ddot{w}\, \delta w\, dx + \\
&\sum_{k=1}^{n}\sum_{m=1}^{n} \int_x \left(D_{11}^{km} \frac{\partial u^m}{\partial x} \frac{\partial \delta u^k}{\partial x} + D_{55}^{km}\, u^m\, \delta u^k \right) dx + \\
&\sum_{k=1}^{n} \int_x B_{55}^{k} \left(\frac{\partial w}{\partial x}\, \delta u^k + u^k \frac{\partial \delta w}{\partial x} \right) dx + \int_x A_{55} \frac{\partial w}{\partial x} \frac{\partial \delta w}{\partial x}\, dx + \\
&\sum_{k=1}^{n}\sum_{m=1}^{n} \int_x E_{31}^{km} \left(\phi^m \frac{\partial \delta u^k}{\partial x} + \frac{\partial u^m}{\partial x}\, \delta \phi^k \right) dx - \\
&\sum_{k=1}^{n}\sum_{m=1}^{n} \int_x G_{33}^{km}\, \phi^m\, \delta \phi^k\, dx - \sum_{k=1}^{n} \int_x \left(f_{1,th}^{k} \frac{\partial \delta u^k}{\partial x} - q_{th}^{k}\, \delta \phi^k \right) dx \\
&= \sum_{k=1}^{n} \left[f_1^k\, \delta u^k + q^k\, \delta \phi^k \right]_x + \left[f_3\, \delta w \right]_x
\end{aligned} \tag{16}$$

The discrete layer laminate matrices for the density, stiffness, piezoelectric, electric permittivitty, and external forces of a composite beam have been presented previously in a general form by Saravanos and Heyliger (1994) and are included for the specific case of a constant through-the-thickness displacement beam in Appendix B. The newly derived resultant laminate thermal force vector is

$$f^{k}_{1,th} = \sum_{l=1}^{L} \int_{z} b\ \lambda_1\ \theta^{l}\ \psi^{j}(z)\ \psi^{k}(z)\ dz \tag{17}$$

and the resultant thermal electric displacement is

$$q^{k}_{th} = \sum_{l=1}^{L} \int_{z} b\ p_3\ \theta^{l}\ \psi^{j}(z)\ \frac{\partial \psi^{k}(z)}{\partial z}\ dz \tag{18}$$

where b is the width of the beam and L is the number of plies.

Finite Element Formulation

The finite element formulation for a composite piezoelectric beam is obtained by incorporating additional local in-plane approximations to the state variables

$$u(x,z,t) = \sum_{i=1}^{m} \sum_{j=1}^{n} U^{ji}(t)\ R^{i}(x)\ \psi^{j}(z) \tag{19}$$

$$w(x,z,t) = \sum_{i=1}^{m} \sum_{j=1}^{n} W^{ji}(t)\ R^{i}(x)\ \psi^{j}(z) \tag{20}$$

$$\phi(x,z,t) = \sum_{i=1}^{m} \sum_{j=1}^{n} \phi^{ji}(t)\ R^{i}(x)\ \psi^{j}(z) \tag{21}$$

where m is the number of in-plane shape functions R. Currently, R is represented using linear Lagrangian interpolation functions and a selectively reduced integration scheme is implemented for the second stiffness term (containing D_{55}) of Eq. (16) in order to eliminate overstiffening at low thicknesses.

By combining Eqs. (3), (7), (8), (10), (19)-(21), the following finite element matrix formulation is obtained for the case of a constant through-the-thickness displacement beam

$$\begin{bmatrix} [M_{11}] & 0 & 0 \\ 0 & [M_{33}] & 0 \\ 0 & 0 & 0 \end{bmatrix} \begin{Bmatrix} \{\ddot{U}\} \\ \{\ddot{W}\} \\ \{\ddot{\Phi}\} \end{Bmatrix} + \begin{bmatrix} [K_{11}] & [K_{13}] & [K_{14}] \\ [K_{31}] & [K_{33}] & 0 \\ [K_{41}] & 0 & [K_{44}] \end{bmatrix} \begin{Bmatrix} \{U\} \\ \{W\} \\ \{\Phi\} \end{Bmatrix} = \begin{Bmatrix} \{F_1\} \\ \{F_3\} \\ \{Q\} \end{Bmatrix} + \begin{Bmatrix} \{F_{1,th}\} \\ 0 \\ \{Q_{th}\} \end{Bmatrix} \tag{22}$$

where the elements of the sub matrices above are calculated from the generalized discrete layer laminate matrices defined previously in Appendix B and in Eqs. (17-18). The finite element matrices for the mass, stiffness, and external force have been presented in a general form by Saravanos and Heyliger (1994) and are included in Appendix C for the specific case of a constant through-the-thickness displacement beam. The newly derived finite element thermal force vector is

$$F^i_{1,th} = \int_x f_{1,th} \frac{\partial R^i(x)}{\partial x} \, dx \tag{23}$$

and the thermal electric displacement is

$$Q^i_{th} = - \int_x q_{th} \, R^i(x) \, dx \tag{24}$$

The coupled finite element formulation can also be expressed in a compact form as

$$\begin{bmatrix} [M_{uu}] & 0 \\ 0 & 0 \end{bmatrix} \begin{Bmatrix} \{\ddot{U}\} \\ \{\ddot{\Phi}\} \end{Bmatrix} + \begin{bmatrix} [K_{uu}] & [K_{u\phi}] \\ [K_{\phi u}] & [K_{\phi\phi}] \end{bmatrix} \begin{Bmatrix} \{U\} \\ \{\Phi\} \end{Bmatrix} = \begin{Bmatrix} \{F\} \\ \{Q\} \end{Bmatrix} + \begin{Bmatrix} \{F_{th}\} \\ \{Q_{th}\} \end{Bmatrix} \tag{25}$$

The electric potential vector in Eq. (25) can be further partitioned into active and sensory components such that $\{\phi\} = \{\phi^a; \phi^s\}$ in order to obtain

$$\begin{bmatrix} [M_{uu}] & 0 \\ 0 & 0 \end{bmatrix} \begin{Bmatrix} \{\ddot{U}\} \\ \{\ddot{\Phi}^s\} \end{Bmatrix} + \begin{bmatrix} [K_{uu}] & [K_{u\phi}^{ss}] \\ [K_{\phi u}^{ss}] & [K_{\phi\phi}^{ss}] \end{bmatrix} \begin{Bmatrix} \{U\} \\ \{\Phi^s\} \end{Bmatrix} = \tag{26}$$

$$\begin{Bmatrix} \{F\} + \{F_{th}\} - [K_{u\phi}^{sa}] \{\Phi^a\} \\ \{Q^s\} + \{Q_{th}\} - [K_{\phi\phi}^{sa}] \{\Phi^a\} \end{Bmatrix}$$

where the superscripts s and a indicate the partitioned submatrices in either sensory or active configuration respectively. This form has the advantage of positioning the unknown variables (displacements and sensory electric potentials) in the left-hand terms, while the known quantities (mechanical loads, thermal loads, electric charges, and active voltages) are included in the right-hand terms.

Eq. (26) can then be uncoupled into the following independent equations for the structural displacements

$$[M_{uu}] \{\ddot{U}\} + ([K_{uu}] - [K_{u\phi}^{ss}] [K_{\phi\phi}^{ss}]^{-1} [K_{\phi u}^{ss}]) \{U\} = \{F\} + \tag{27}$$

$$\{F_{th}\} + ([K_{u\phi}^{ss}] [K_{\phi\phi}^{ss}]^{-1} [K_{\phi\phi}^{sa}] - [K_{u\phi}^{sa}]) \{\Phi^a\}$$

and the electric potentials at the sensors

$$\{\Phi^s\} = -[K_{\phi\phi}^{ss}]^{-1} ([K_{\phi u}^{ss}] \{U\} + [K_{\phi\phi}^{sa}] \{\Phi^a\} - \{Q^s\} - \{Q_{th}\}) \tag{28}$$

Applications

Materials and Assumptions

Results from representative problems are presented in this section to evaluate the discrete layer formulation and to demonstrate the performance of simple sensory/active structures in thermal environments. Two different composite cantilever beam configurations are considered as shown in Figures 1(a) and 1(b). For both cases, the beam is 25.4 cm (10 in) long and consists of various orientations of graphite/epoxy plies attached to piezoelectric layers, where each graphite/epoxy ply and piezoelectric layer has a thickness of 0.0127 cm (0.005 in). A total of 30 equally spaced linear beam elements are modeled along the length of the beam, while one discrete layer is used through-the-

thickness for each piezoelectric and graphite/epoxy layer as shown in Figure 2(a). The room temperature material properties used for the graphite/epoxy and piezoelectric layers are listed in Table I. The piezoelectric material used for this study is the commercially available piezoceramic APC 840 (American Piezo Ceramics Inc.), while representative material properties of a graphite/epoxy composite were selected. The current study uses the constant through-the-thickness displacement beam theory and neglects the temperature dependence of material properties.

[0_8/p] Beam Under Uniform Thermal Load

Thermal Displacements. The first beam considered is a [0_8/p] configuration, where p represents the piezoelectric layer, under a uniform thermal load of 100°C. The presence of the piezoelectric layer results in an asymmetric laminate configuration, which induces thermal distortions under the thermal load. Figures 3 and 4 illustrate the induced axial and transverse displacements produced when the beam is operating in closed circuit conditions. The closed circuit condition is obtained by grounding (0 Volts) both the lower and upper surfaces of the piezoelectric layer. Grounding both surfaces effectively eliminates the induced piezoelectric strains and produces a virtually conventional composite beam. Thus, the results for this grounded loop condition can also be validated using a conventional finite element structural analysis. This conventional finite element analysis was performed using the MARC analysis code (MARC Analysis Research Corporation) with nine layers of 15 eight-noded quadratic plane stress quadrilateral elements as shown in Figure 2(b). Both methods result in almost identical axial and transverse thermal displacements, as shown in Figures 3 and 4, lending credence to the accuracy of the current formulation.

The resultant thermal deflections of the [0_8/p] beam under the open circuit or sensory conditions (only the lower surface of the piezoelectric layer is grounded) are shown in Figures 5 and 6. Since only the lower surface is grounded, the effects of the piezoelectrically induced strains are no longer neutralized and leads to the formation of a sensory electric potential on the top surface as a result of the induced thermal stresses. Figure 6 shows a significant difference ($\sim$15 %) in the transverse displacement between the closed and open circuit conditions. This demonstrates the importance of including the thermo-electrical coupling to model the behavior of thermal piezoelectric structures and illustrates the ability of the mechanics to capture this phenomena.

Sensory Voltage. The open loop case also demonstrates an important potential application of sensory structures in the monitoring of thermal distortions. In these applications, the displacement fields which arise under thermal loadings may be sensed through correlation with the measured voltages at the sensors. This capability is demonstrated in

Figure 7, which shows the measured electric potential (from both the thermal strain and pyroelectric effects) on the top surface corresponding to the axial and transverse displacements shown in Figures 5 and 6. The thermal strain sensory voltage accounts for the effects arising from the thermally induced deformations, while the pyroelectric voltage quantifies the effects that occur due to the variation in temperatures. This application demonstrates the capability to monitor the thermal displacements via the different sensory voltages, which will provide the inferred essential feedback required for thermal distortion management of smart composite structures.

Thermal Distortion Management. The capability to actively compensate for thermal distortions is demonstrated in Figure 8 for the $[0_8/p]$ beam. Through application of a voltage differential between the upper and lower surfaces of the piezoelectric layer, the converse piezoelectric effect can be utilized to compensate for the thermal displacements. As shown in the figure, the thermal displacement behavior of the beam can be completely altered from the open loop state depending on the value of the voltage differential. The thermal distortion can be eliminated by applying a voltage differential of 300 V, while a completely opposite curvature of the beam can be obtained by applying a voltage differential of 500 V. These results indicate the potential of piezoelectric structures to suppress thermally induced bending.

$[p/0/90/\pm45]_s$ Beam Under Thermal Gradient

The present example considers multiple piezoelectric layers (to simultaneously take advantage of both the sensory and active behavior of piezoelectric materials), a more general lamination $[p/0/90/\pm45]_s$, and a through-the-thickness linear thermal gradient (120°C on the top surface and 20°C on the bottom surface) as shown in Figure 1(b). Even though the beam has a symmetric laminate configuration including the piezoelectric layers, the applied thermal gradient produces a bending deflection in the beam.

Thermal Displacements. The induced axial and transverse displacements produced in the beam when both piezoelectric layers are operating in closed circuit conditions is shown in Figures 9 and 10. Also shown are the results from a conventional finite element analysis performed using the MARC analysis code (MARC Analysis Research Corporation) with ten layers of 15 eight-noded quadratic plane stress quadrilateral elements. Both methods lead to identical predictions, lending credence to the validity to the current formulation.

Combined Sensory and Actuator Application. In this application, the upper piezoelectric layer is assumed to act as the sensor to monitor the induced electric potential, while the lower piezoelectric layer is used to actively compensate thermal deflections. Figures 11 and 12 show the axial and transverse deflections of the beam under applied voltages of 0

V, 100 V, and 200 V on the active (lower) piezoelectric layer. As shown in the figures, increasing the applied voltage reduces the thermally induced deflections from the reference state (0 V). The corresponding sensory electric potentials (from both the thermal strain and pyroelectric effects) measured on the upper piezoelectric layer (sensor) for the different active voltages are shown in Figure 13. In actual applications, a control loop would be established between the sensory and active layer, to monitor the sensory voltages and then to generate the appropriate active voltage which will minimize the thermal distortions. This capability is planned to be investigated in the near future.

Convergence Studies

The accuracy of the beam element developed in this study is verified for both beam configurations examined. The open circuit condition case is used for the $[0_8/p]$ beam, while the 100 V active voltage case is used for the $[p/0/90/\pm45]_s$ beam. The results are shown in Table II and indicates the relative insensitivity of this element to the varying aspect ratios for the configurations examined.

Summary

The development of discrete layer mechanics to model the coupled thermoelectro-mechanical response of smart thermal composite beams with embedded piezoelectric layers was described. The corresponding finite element formulation was presented and a linear layerwise beam element developed. The capability of the updated mechanics to capture the response of piezoelectric composite structures under a thermal environment was demonstrated through numerical examples performed on a graphite/epoxy beam with attached piezoelectric layers. For the numerical study, a constant through-the-thickness displacement beam theory was used and the temperature dependence of material properties neglected. Predicted results for the beam in closed circuit conditions were validated using a conventional finite element analysis.

Applications of the active and sensory modes operating independently were demonstrated on a $[0_8/p]$ beam under a uniform thermal load of 100°C, while the combined active and sensory operations of a $[p/0/90/\pm45]_s$ beam under a thermal gradient was illustrated. The numerical studies indicate the significance of thermal effects for smart piezoelectric structures and illustrate the strong coupling between thermal and piezoelectric effects under open circuit conditions. Overall, the case studies have demonstrated the capabilities of the current mechanics to represent the complicated thermo-mechanical response of thermal smart structures.

Nomenclature:

$[A^{mn}]$, $[B^{mn}]$, $[D^{mn}]$	generalized laminate matrices
[C]	elastic stiffness
[d]	piezoelectric tensor
{D}	electric displacement vector
[e]	piezoelectric tensor
{E}	electric field
$[E^{mn}]$	generalized laminate piezoelectric matrices
{f}	generalized laminate thermal force vector
$\{ \bar{f}_i \}$	body force per unit volume
{F}	thermal force vector
$[G^{mn}]$	generalized laminate electric permittivity matrices
[K]	stiffness matrix
[M]	mass matrix
p	pyroelectric constant
$[P^{mn}]$	generalized laminate mass matrices
{q}	generalized laminate thermal electric displacements
$\bar{q}$	surface electric charge
{Q}	thermal electric displacements

R	in-plane interpolation functions
[s]	elastic compliance
{S}	engineering strain
t	time
$\{ \bar{t} \}$	surface tractions
T	temperature
u, v, w	displacements along x, y, z axes, respectively
x, y, z	structural axes
x_1, x_2, x_3	material axes
α	strain coefficient of thermal expansion
δ	variational operator
$[\epsilon]$	electric permittivity tensor
λ	stress coefficient of thermal expansion
ψ	through-the-thickness interpolation function
ϕ	electric potential
ρ	density
$\{\sigma\}$	mechanical stress
θ	temperature difference from reference temperature

Superscripts:

E	constant electric field conditions
S	constant strain conditions
T	constant temperature conditions
σ	constant stress conditions
a	active
s	sensory

Subscripts:

l	layer or ply
o	reference conditions
uu, uϕ, $\phi\phi$	structural, piezoelectric, and dielectric, respectively

References

Allik, H. and Hughes, T.J.R., "Finite Element Method for Piezoelectric Vibration," International Journal for Numerical Methods in Engineering, Vol. 2, pp. 151-157, 1970.

American Piezo Ceramics, Inc., Mackeyville, PA.

Bailey, T. and Hubbard, J.E., "Distributed Piezoelectric-Polymer Active Vibration Control of a Cantilever Beam," J. Guidance, Vol. 8, No. 5, pp. 605-611, 1985.

Crawley, E.F. and deLuis, J., "Use of Piezoelectric Actuators as Elements of Intelligent Structures," AIAA Journal, Vol. 25, No. 10, pp. 1373-1385, 1987.

Ha, S.K., Keilers, C., and Chang, F.-K., "Finite Element Analysis of Composite Structures Containing Distributed Piezoceramic Sensors and Actuators," AIAA Journal, Vol. 30, No. 3, pp. 772-780, 1992.

Heyliger, P., Ramirez G. and Saravanos D. A., "Coupled Discrete Layer Finite Elements for Laminated Piezoelectric Plates," Communications in Numerical Methods in Engineering, Vol. 10, pp. 971-981, 1994.

Lammering, R., "The Application of a Finite Shell Element for Composites Containing Piezoelectric Polymers in Vibration Control," Computers and Structures, Vol. 41, pp. 1101-1109, 1991.

Lee, C.-K., Chiang, W.-W., and O'Sullivan, T.C., "Piezoelectric Modal Sensor/Actuator Pairs for Critical Active Damping Vibration Control," J. Acoust. Soc. Am., Vol. 90, No. 1, pp. 374-384, 1991.

MARC Reference Library Volumes A-D, Version K 5.2, MARC Analysis Research Corporation, Palo Alto, CA, 1992.

Mindlin, R.D., "Equations of High Frequency Vibrations of Thermopiezoelectric Crystal Plates," International Journal of Solids Structures, Vol. 10, pp. 625-632, 1974.

Naillon, M., Coursant, R.H., and Besnier, F., "Analysis of Piezoelectric Structures by a Finite Element Method," ACTA Electronica, Vol. 25, No. 4, pp. 341-362, 1983.

Nye, J.F., Physical Properties of Crystals, The Clarendon Press, Oxford, 1964.

Rao, S.S. and Sunar, M., "Analysis of Distributed Thermopiezoelectric Sensors and Actuators in Advanced Intelligent Structures," AIAA Journal, Vol. 31, No. 7, pp. 1280-1286, 1993.

Reddy, J.N., "A Generalization of Two-Dimensional Theories of Laminated Composite Plates," Communications in Applied Numerical Methods, Vol. 3, pp. 173-180, 1987.

Robbins, D.H. and Reddy, J.N., "Analysis of Piezoelectrically Actuated Beams Using a Layer-Wise Displacement Theory," Computers and Structures, Vol. 41, pp. 265-279, 1991.

Saravanos D.A. and Heyliger P.R. "Coupled Electromechanical Response of Composite Beams with Embedded Piezoelectric Sensors and Actuators," Journal of Intelligent Material Systems and Structures, to appear; also NASA CR 195313, 1994.

Tauchert, T.R., "Piezothermoelastic Behavior of a Laminated Plate," Journal of Thermal Stresses, Vol. 15, pp. 25-37, 1992.

Tzou, H.S. and Gadre, M., "Theoretical Analysis of a Multi-Layered Thin Shell Coupled with Piezoelectric Shell Actuators for Distributed Vibration Controls," Journal of Sound and Vibration, Vol. 132, No. 3, pp. 433-450, 1989.

Tzou, H.S. and Howard, R.V., "A Piezothermoelastic Thin Shell Theory Applied to Active Structures," Journal of Vibration and Acoustics, Vol. 116, pp. 295-302, 1994.

Tzou, H.S. and Tseng, C.I., "Distributed Piezoelectric Sensor/Actuator Design for Dynamic Measurement/Control of Distributed Parametric Systems: A Piezoelectric Finite Element Approach," Journal of Sound and Vibration, Vol. 138, pp. 17-34, 1990.

Tzou, H.S. and Ye, R., "Piezothermoelasticity and Precision Control of Piezoelectric Systems: Theory and Finite Element Analysis," Journal of Vibration and Acoustics, Vol. 116, pp. 489-495, 1994.

Wang, B.-T. and Rogers, C.A., "Laminate Plate Theory for Spatially Distributed Induced Strain Actuators," Journal of Composite Materials, Vol. 25, pp. 433-452, 1991.

Table I. - Room Temperature Material Properties of Piezoelectric Composite Beam

Property	Graphite/Epoxy	Piezoceramic APC 840 (APC, Inc.)
Density, ρ, g/cm^3 (lb/in^3)	2.1 (0.076)	7.60 (0.27)
Elastic Modulus, E_{11}, GPa (Msi)	39 (5.7)	68 (10.0)
Elastic Modulus, E_{22}, GPa (Msi)	8.6 (1.24)	---
Shear Modulus, G_{12}, GPa (Msi)	3.8 (0.54)	26.2 (3.84)
Major Poisson's Ratio, ν_{12}	0.28	0.30
Minor Poisson's Ratio, ν_{21}	0.06	---
Thermal Expansion Coefficient, α_{11}, 10^{-6}/°C (10^{-6}/°F)	7.0 (3.9)	3.8 (2.1)
Thermal Expansion Coefficient, α^{22}, 10^{-6}/°C (10^{-6}/°F)	21.0 (11.7)	---
Piezoelectric Charge Constant, d_{31}, 10^{-12} m/V	---	-125.
Electric Permittivity, ϵ_{33}, 10^{-9} N/V^2	---	11.06
Pyroelectric Constant, p_3, 10^{-3} C/(m^2 °C)	---	-0.25

Table II. - Convergence Studies of Beam Element

Aspect Ratio	$[0_8/p]$ Open Loop Case		$[0/90/\pm45]_s$ 100 V Case	
	u	w	u	w
400	2.01475 e-4	8.42061 e-3	1.43711 e-4	1.14907 e-2
200	2.01474 e-4	8.42061 e-3	1.43683 e-4	1.14906 e-2
100	2.01471 e-4	8.42061 e-3	1.43645 e-4	1.14905 e-2
50	2.01468 e-4	8.42059 e-3	1.43632 e-4	1.14905 e-2
25	2.01468 e-4	8.42059 e-3	1.43631 e-4	1.14905 e-2

Appendix A: Constitutive Equations: Constant Through-the-Thickness Displacement

The simplified constitutive equations for constant through-the-thickness displacement are

$$\begin{Bmatrix} S_1 \\ S_5 \end{Bmatrix} = \begin{bmatrix} s_{11} & 0 \\ 0 & s_{55} \end{bmatrix} \begin{Bmatrix} \sigma_1 \\ \sigma_5 \end{Bmatrix} + \begin{bmatrix} 0 & d_{31} \\ 0 & 0 \end{bmatrix} \begin{Bmatrix} E_1 \\ E_3 \end{Bmatrix} + \begin{bmatrix} \alpha_1 \\ 0 \end{bmatrix} \theta \tag{A-1}$$

$$D_3 = d_{31}\ \sigma_1 + \epsilon_{33}\ E_3 + p_3\ \theta \tag{A-2}$$

or in semi-inverted form

$$\begin{Bmatrix} \sigma_1 \\ \sigma_5 \end{Bmatrix} = \begin{bmatrix} C_{11} & 0 \\ 0 & C_{55} \end{bmatrix} \begin{Bmatrix} S_1 \\ S_5 \end{Bmatrix} - \begin{bmatrix} 0 & e_{31} \\ 0 & 0 \end{bmatrix} \begin{Bmatrix} E_1 \\ E_3 \end{Bmatrix} - \begin{bmatrix} \lambda_1 \\ 0 \end{bmatrix} \theta \tag{A-3}$$

$$D_3 = e_{31}\ S_1 + \epsilon_{33}\ E_3 + p_3\ \theta \tag{A-4}$$

Appendix B: Discrete Layer Laminate Matrices: Constant Through-the-Thickness Displacement

The laminate density matrices are

$$P_{11}^{km} = \sum_{l=1}^{L} \int_z b\ \rho\ \psi^k(z)\ \psi^m(z)\ dz \tag{B-1}$$

$$P_{33} = \sum_{l=1}^{L} \int_z b\ \rho\ dz \tag{B-2}$$

the laminate stiffness matrices are

$$A_{55} = \sum_{l=1}^{L} \int_z b\ C_{55}\ dz \tag{B-3}$$

$$B_{55}^{k} = \sum_{l=1}^{L} \int_z b\ C_{55}\ \frac{\partial \psi^k(z)}{\partial z}\ dz \tag{B-4}$$

$$D_{11}^{km} = \sum_{l=1}^{L} \int_z b\ C_{11} \psi^k(z)\ \psi^m(z)\ dz \tag{B-5}$$

$$D_{55}^{km} = \sum_{l=1}^{L} \int_z b\ C_{55}\ \frac{\partial \psi^k(z)}{\partial z}\ \frac{\partial \psi^m(z)}{\partial z}\ dz \tag{B-6}$$

the piezoelectric laminate matrix is

$$E_{31}^{km} = \sum_{l=1}^{L} \int_z b\ e_{31}\ \psi^k(z)\ \frac{\partial \psi^m(z)}{\partial z}\ dz \tag{B-7}$$

the dielectric permittivity laminate matrix is

$$G_{33}^{km} = \sum_{l=1}^{L} \int_z b\, e_{33}\, \frac{\partial \psi^k(z)}{\partial z}\, \frac{\partial \psi^m(z)}{\partial z}\, dz \qquad \text{(B-8)}$$

the external forces are

$$f_1^k = \sum_{l=1}^{L} \int_z b\, \bar{t}_1\, \psi^k(z)\, dz \qquad \text{(B-9)}$$

$$f_3 = \sum_{l=1}^{L} \int_z b\, \bar{t}_3\, dz \qquad \text{(B-10)}$$

$$q^k = \sum_{l=1}^{L} \int_z b\, \bar{q}\, \psi^k(z)\, dz \qquad \text{(B-11)}$$

where L is the number of plies.

Appendix C: Finite Element Matrices: Constant Through-the-Thickness Displacement

The mass matrices are

$$M_{11}^{ij} = \int_x P_{11}\, R^i(x)\, R^j(x)\, dx \tag{C-1}$$

$$M_{33}^{ij} = \int_x P_{33}\, R^i(x)\, R^j(x)\, dx \tag{C-2}$$

The stiffness matrices are

$$K_{11}^{ij} = \int_x \{\, D_{11}\, \frac{\partial R^i(x)}{\partial x}\, \frac{\partial R^j(x)}{\partial x} + D_{55}\, R^i(x)\, R^j(x) \,\}\, dx \tag{C-3}$$

$$K_{13}^{ij} = \int_x B_{55}\, R^i(x)\, \frac{\partial R^j(x)}{\partial x}\, dx \tag{C-4}$$

$$K_{14}^{ij} = \int_x E_{31}\, R^i(x)\, \frac{\partial R^j(x)}{\partial x}\, dx \tag{C-5}$$

$$K_{33}^{ij} = \int_x A_{55}\, \frac{\partial R^i(x)}{\partial x}\, \frac{\partial R^j(x)}{\partial x}\, dx \tag{C-6}$$

$$K_{44}^{ij} = -\int_x G_{33}\, R^i(x)\, R^j(x)\, dx \tag{C-7}$$

The external force vectors are

$$F_1^i = [\, f_1 \; R^i(x) \,]_x \tag{C-8}$$

$$F_3^i = [\, f_3 \; R^i(x) \,]_x \tag{C-9}$$

$$Q^i = [\, q \; R^i(x) \,]_x \tag{C-10}$$

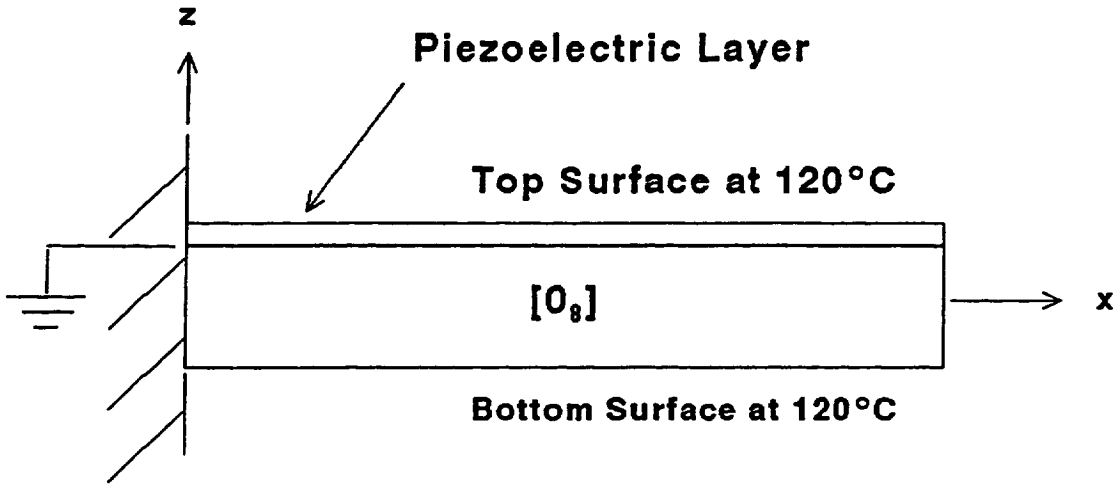

Figure 1(a):[0$_8$/p] Beam Under A Uniform Thermal Load (100°C)

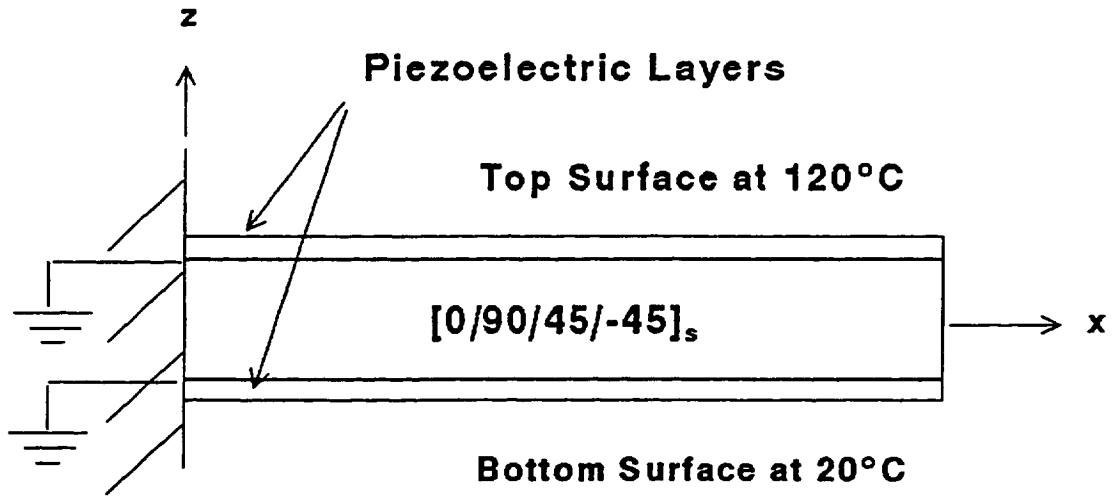

Figure 1(b):[p/0/90/±45]$_s$ Beam Under A Thermal Gradient

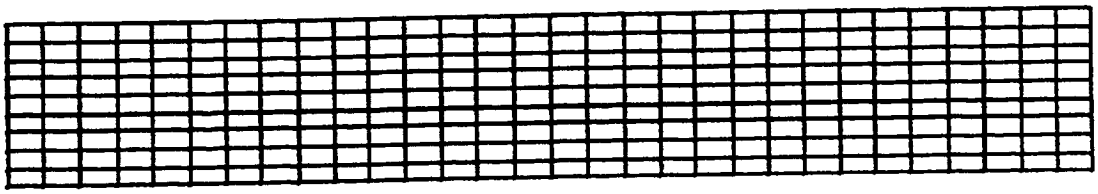

Figure 2(a): [0_s/p] Beam Mesh for Developed Finite Element Program

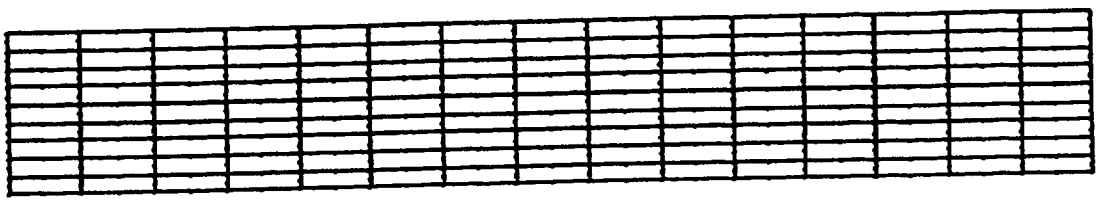

Figure 2(b): [0_s/p] Beam Mesh for Conventional Finite Element Program

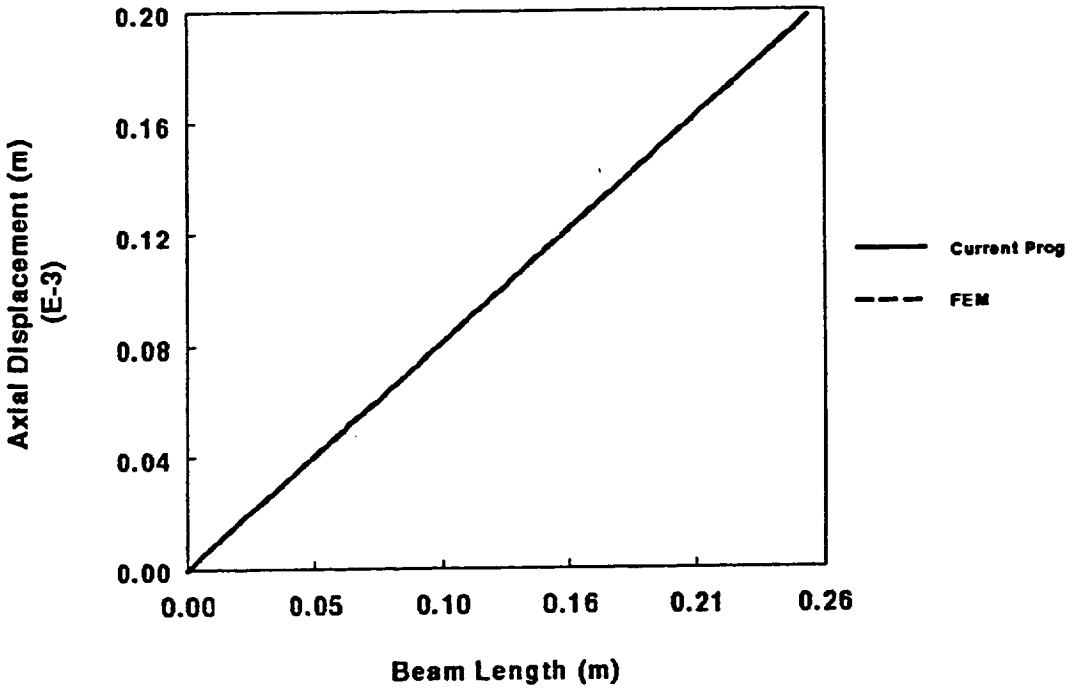

Figure 3: Axial Displacement of a [0_g/p] Beam Under A Uniform Thermal Load (100°C) in Closed Circuit Conditions

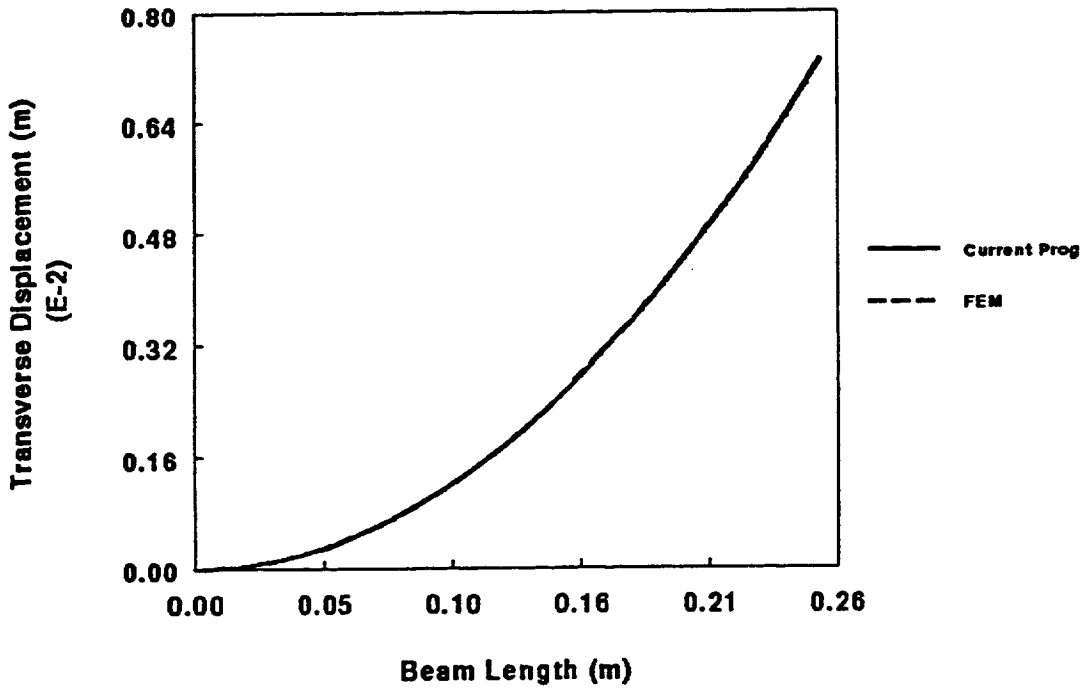

Figure 4: Transverse Displacement of a [0_g/p] Beam Under A Uniform Thermal Load (100°C) in Closed Circuit Conditions

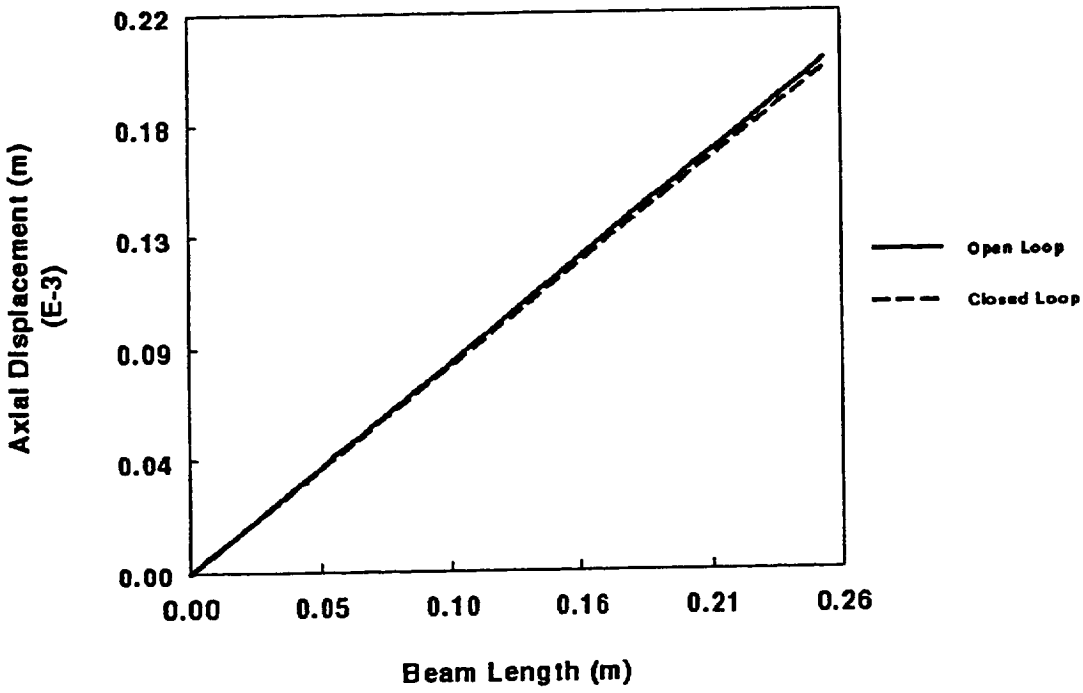

Figure 5: Axial Displacement Comparisons of a [0_s/p] Beam Under A Uniform Thermal Load (100°C) in Open and Closed Circuit Conditions

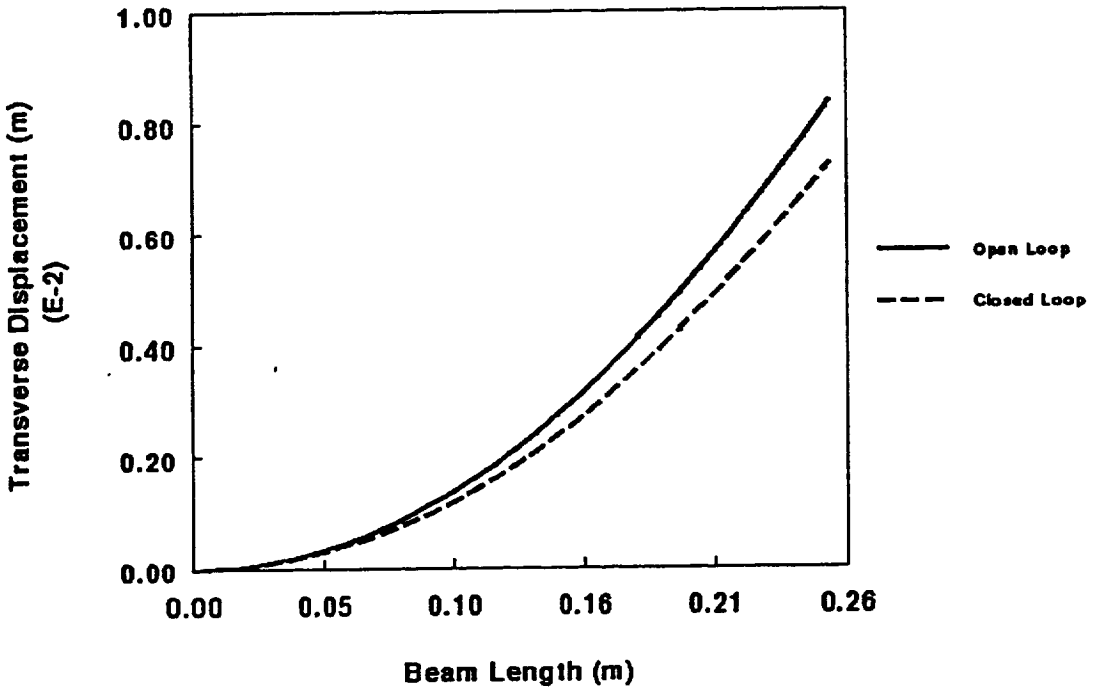

Figure 6: Transverse Displacement Comparisons of a [0_s/p] Beam Under A Uniform Thermal Load (100°C) in Open and Closed Circuit Conditions

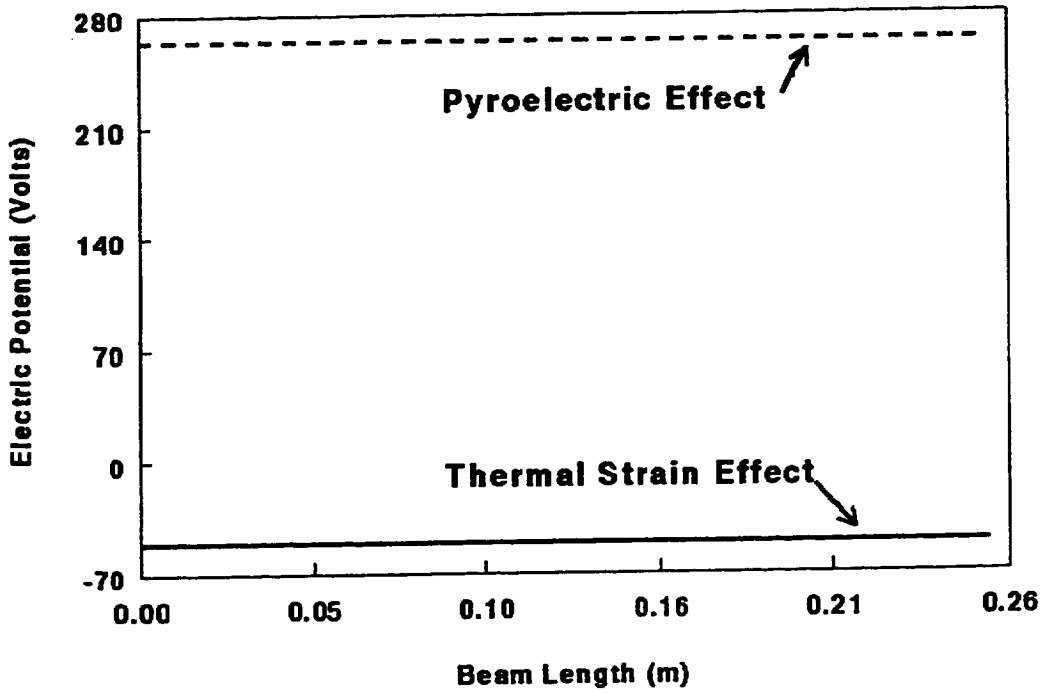

Figure 7: Measured Sensory Electric Potential of a [0_s/p] Beam Under A Uniform Thermal Load (100°C)

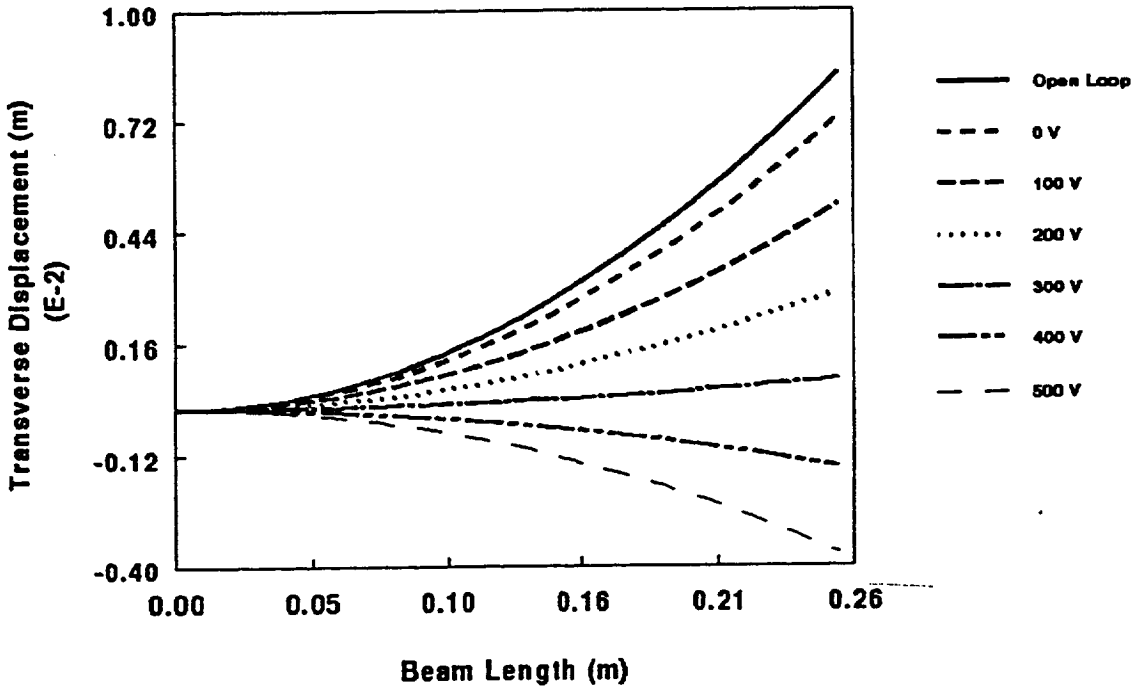

Figure 8:Active Compensation of the Transverse Displacement of a [0_s/p] Beam Under A Uniform Thermal Load (100°C)

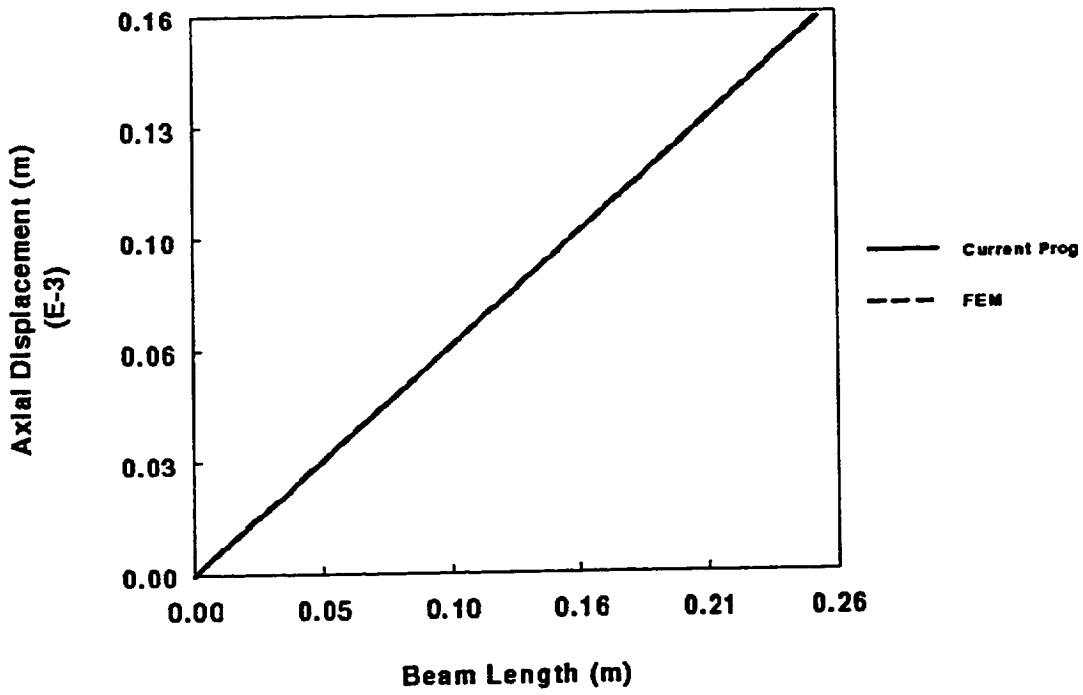

Figure 9: Axial Displacement of a $[p/0/90/\pm45]_s$ Beam Under A Thermal Gradient in Closed Circuit Conditions

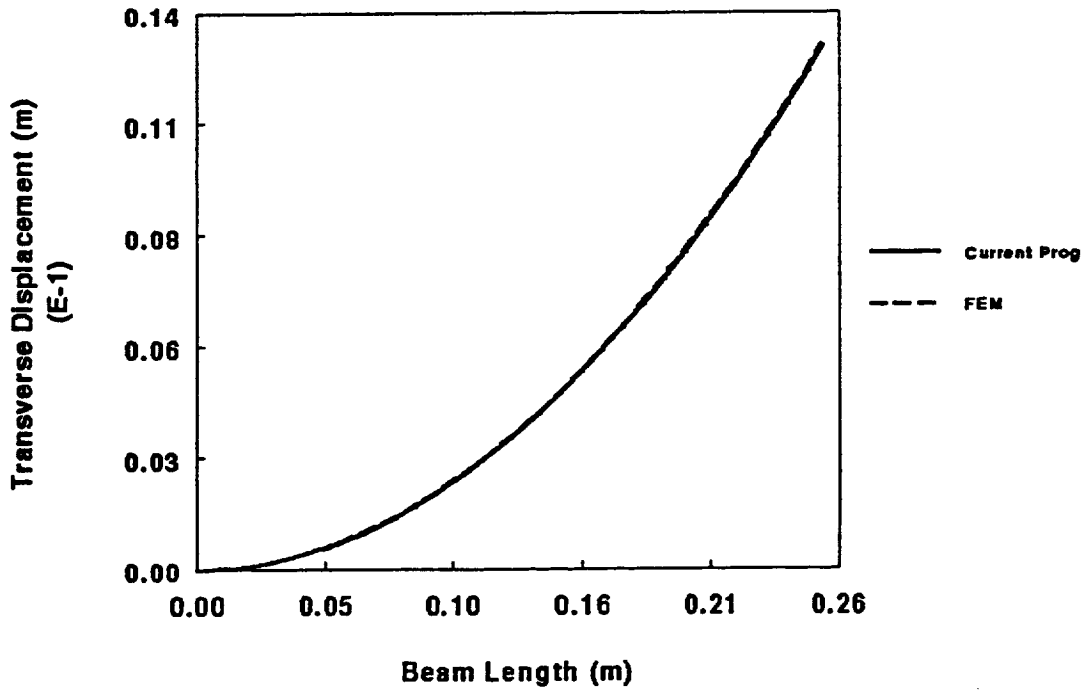

Figure 10: Transverse Displacement of a $[p/0/90/\pm45]_s$ Beam Under A Thermal Gradient in Closed Circuit Conditions

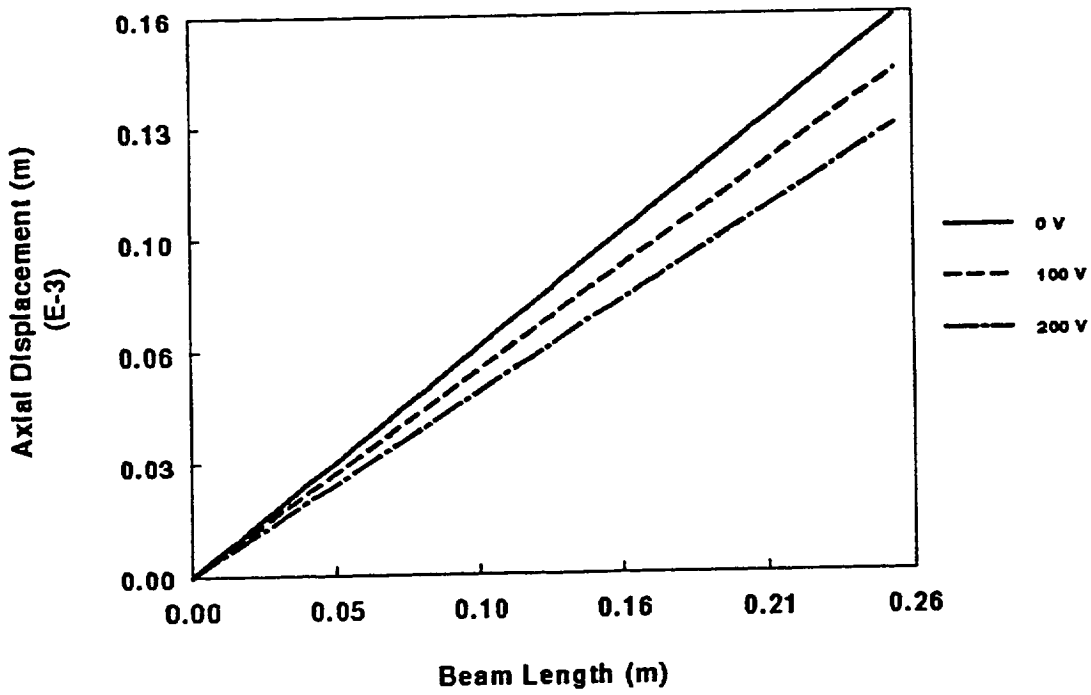

Figure 11: Active Compensation of the Axial Displacement of a $[p/0/90/\pm45]_s$ Beam Under A Thermal Gradient

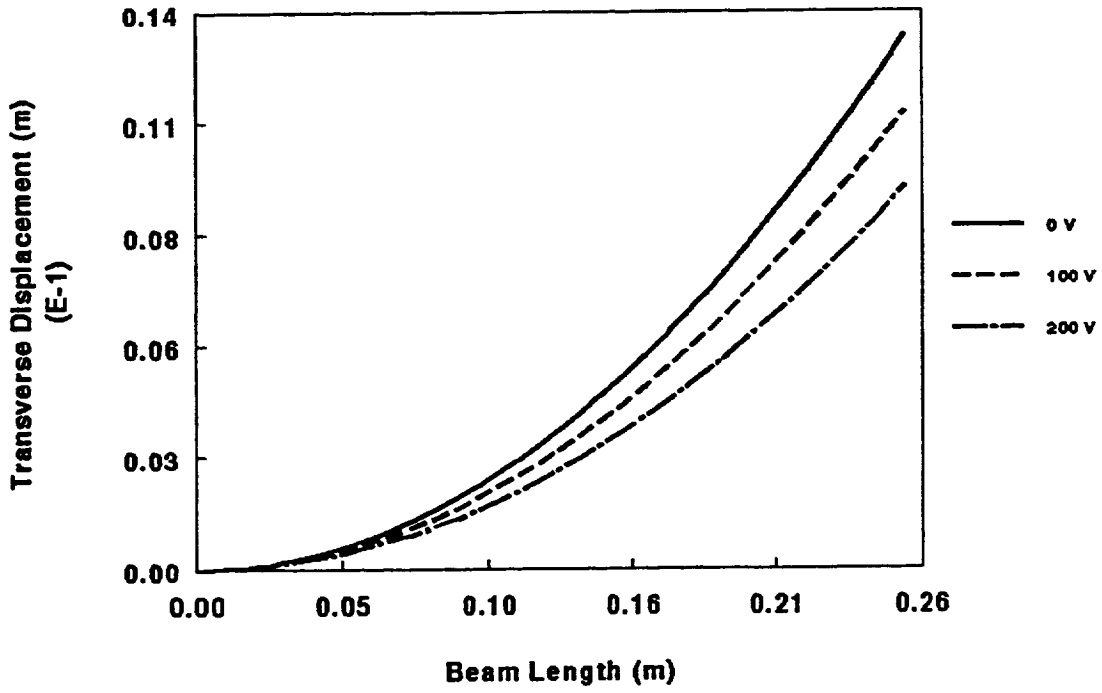

Figure 12: Active Compensation of the Transverse Displacement of a $[p/0/90/\pm45]_s$ Beam Under A Thermal Gradient

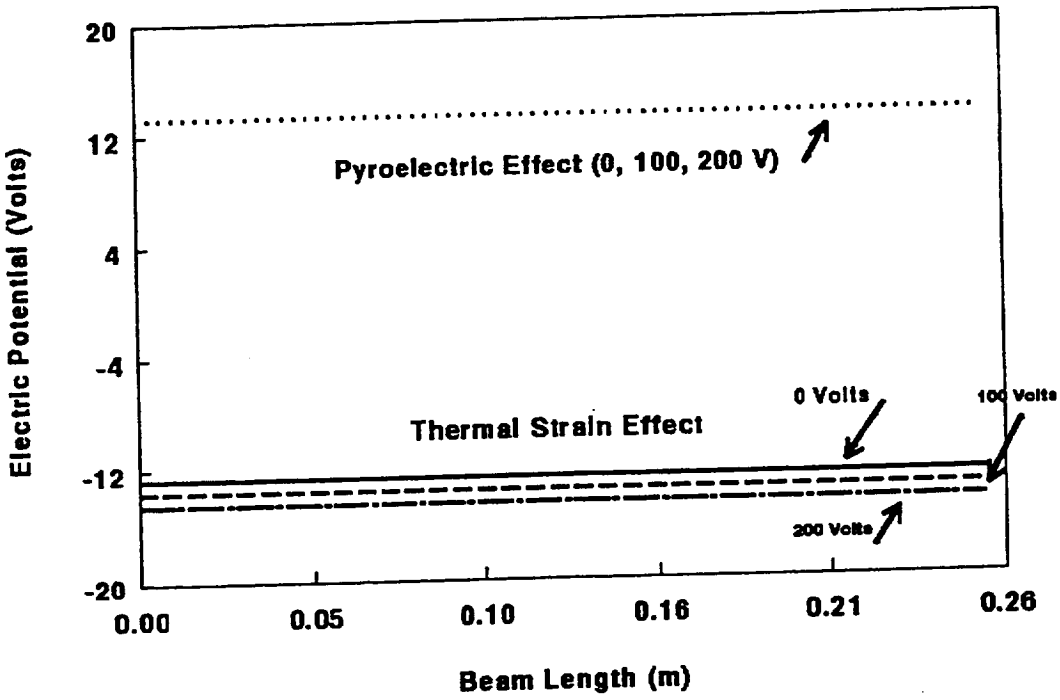

Figure 13: Measured Sensory Electric Potential of a $[p/0/90/\pm45]_s$ Beam Under A Thermal Gradient

REPORT DOCUMENTATION PAGE

Form Approved
OMB No. 0704-0188

1. AGENCY USE ONLY (*Leave blank*)	2. REPORT DATE	3. REPORT TYPE AND DATES COVERED
	March 1995	Technical Memorandum

4. TITLE AND SUBTITLE

A Coupled Layerwise Analysis of the Thermopiezoelectric Response of Smart Composite Beams

5. FUNDING NUMBERS

WU-505-63-5B

6. AUTHOR(S)

H.-J. Lee and D.A. Saravanos

7. PERFORMING ORGANIZATION NAME(S) AND ADDRESS(ES)

National Aeronautics and Space Administration
Lewis Research Center
Cleveland, Ohio 44135-3191

8. PERFORMING ORGANIZATION REPORT NUMBER

E-9528

9. SPONSORING/MONITORING AGENCY NAME(S) AND ADDRESS(ES)

National Aeronautics and Space Administration
Washington, D.C. 20546-0001

10. SPONSORING/MONITORING AGENCY REPORT NUMBER

NASA TM-106889
AIAA-95-1101

11. SUPPLEMENTARY NOTES

Prepared for the 36th Structures, Structural Dynamics, and Materials Conference cosponsored by AIAA, ASME, AHS, and ASC, New Orleans, Louisiana, April 10-13, 1995. H.-J. Lee, NASA Lewis Research Center; D.A. Saravanos, Ohio Aerospace Institute, Cleveland, Ohio 44142 and NASA Resident Research Associate at Lewis Research Center. Responsible person, H.-J. Lee, organization code 5210, (216) 433-3316.

12a. DISTRIBUTION/AVAILABILITY STATEMENT

Unclassified - Unlimited
Subject Category 24

This publication is available from the NASA Center for Aerospace Information, (301) 621-0390.

12b. DISTRIBUTION CODE

13. ABSTRACT (***Maximum 200 words***)

Thermal effects are incorporated into previously developed discrete layer mechanics for piezoelectric composite beam structures. The updated mechanics explicitly account for the complete coupled thermoelectromechanical response of smart composite beams. This unified representation leads to an inherent capability to model both the sensory and actuator responses of piezoelectric composite beams in a thermal environment. Finite element equations are developed and numerical results are presented to demonstrate the capability of the current formulation to represent the behavior of both sensory and active smart structures under thermal loadings.

14. SUBJECT TERMS

Composites; Laminates; Piezoelectrics; Thermopiezoelectrics; Adaptive structures; Smart materials; Structures; Beams; Sensors; Actuators

15. NUMBER OF PAGES

39

16. PRICE CODE

A03

17. SECURITY CLASSIFICATION OF REPORT	18. SECURITY CLASSIFICATION OF THIS PAGE	19. SECURITY CLASSIFICATION OF ABSTRACT	20. LIMITATION OF ABSTRACT
Unclassified	Unclassified	Unclassified	

National Aeronautics and
Space Administration

Lewis Research Center
21000 Brookpark Rd.
Cleveland, OH 44135-3191